

## Auger-electron-spectroscopy analysis of chemical states in ion-beam-deposited carbon layers on graphite

H. J. Steffen, C. D. Roux, D. Marton, and J. W. Rabalais

*Department of Chemistry, University of Houston, Houston, Texas 77204-5641*

(Received 10 December 1990; revised manuscript received 12 April 1991)

The mechanism of formation of diamondlike carbon layers at room temperature by ion-beam deposition has been investigated. Mass-selected  $C^+$  ions with kinetic energy between 50 and 150 eV were deposited on cleaved graphite under UHV conditions with a maximum dose of  $\sim 3 \times 10^{17} C^+/cm^2$ . Auger-electron spectroscopy (AES) was used to delineate the carbon chemical states that were formed. Similar experiments with a  $Ne^+$  ion beam revealed the extent of ion-induced defect formation. Factor analysis and least-squares fitting were applied for quantitative evaluation of the different carbon bonding states during film growth. A peak in the high-energy region of the  $KVV$  AES spectrum at  $3.8 \pm 1$  eV below the Auger line threshold is related to the degree of disorder in the different carbon phases. The carbon-layer growth can be described as a two-stage process: First, the graphite lattice is being damaged; then an amorphous network of tetrahedrally ( $sp^3$ ) and trigonally ( $sp^2$ ) coordinated carbon atoms forms.

### I. INTRODUCTION

Among the variety of diamondlike carbon film preparation techniques, those which apply or involve hyperthermal (1–300 eV) ion species in the deposition process show promise in achieving outstanding homogeneous, mechanical, thermal, optical, and chemical layer properties at low substrate temperature.<sup>1</sup> In spite of extensive studies in the past 20 years (for a recent review see, e.g., Refs. 2 and 3) and although films with the diamond structure have been successfully grown, the complex chemical-physical processes in practical systems like plasma and sputter deposition, ion-beam-assisted and plasma-assisted chemical vapor deposition, etc., are not well understood and therefore cannot be completely controlled.<sup>4–6</sup>

The present investigation represents an extension of our previous research on carbon film growth using mass-selected ion-beam deposition (MSIBD) under UHV conditions.<sup>7</sup> MSIBD is unique in its ability to control and independently vary all parameters involved in the film deposition process. These include ion species, energy, incidence angle, and flux, and substrate environment (background gases and temperature), as well as surface state. This makes possible the achievement of a better understanding of the film evolution mechanism and the basic phenomena involved. Electron spectroscopic diagnostics, coupled with parametric investigations of carbon film evolution on different substrate materials at room temperature, allowed the observation<sup>7</sup> of three stages in this process: an initial carbidic stage, an amorphous or graphitelike transition stage, and finally the emergence of diamondlike features. On the basis of these experimental results, supported by classical trajectory simulations using the TRIM computer program code, the subplantation model for film growth from hyperthermal species was developed.<sup>8</sup> According to this model, the processes

occurring upon low-energy ion bombardment of solid surfaces include penetration of the ion species into the subsurface region, stopping due to several energy-loss mechanisms, preferential displacement of atoms with low displacement energy  $E_d$  (leaving the high- $E_d$  atoms intact), and inclusion of a new phase due to incorporation of a high density of interstitials in the host matrix.

In nearly all of our carbon depositions on different substrates, an amorphous or graphiticlike layer evolved as a transition stage.<sup>7</sup> In this study we chose graphite as the substrate material in order to observe the deposition process without any possible influence of heterogeneous substrate materials and their surface states on the final carbon film structure. In addition, it is attractive to elucidate the consequences of ion impact at low energy on an ordered, well-defined carbon structure such as graphite with respect to bond breaking and new bond formation. The impact of low-energy carbon ions on graphite has also been compared to that of neon ions of similar energy and dose. Such comparison allows conclusions to be drawn on the extent of ion-induced lattice damage during deposition. It can consequently help to distinguish between the altered chemical state of carbon due to defect creation as opposed to the formation of a new type of carbon bond.

The ability of AES to provide chemical state information for carbon is well known;<sup>9</sup> the C  $KVV$  Auger line shape for graphite, amorphous carbon, and diamond are characteristically different.<sup>10</sup> The description of the chemical state of carbon in deposited films is, however, frequently confusing, qualitative, and insufficient. For example, the expression “diamondlike” is often used even when the AES line shape does not resemble that of diamond but rather that of amorphous carbon. Sophisticated techniques such as factor analysis and least-squares decomposition allow a more quantitative description and comparison of AES line shapes. Their application can

shed light on the basic growth mechanism, as well as on the resulting structure. This work focuses on AES analysis of different chemical states or carbon bonding types.

## II. EXPERIMENT

The experiments were performed with a system consisting of a low-energy ion-beam line and an UHV deposition chamber with electron spectroscopic facilities which has been described in detail elsewhere.<sup>11</sup> The ions, produced by a Colutron ion source, maintained at 30–300 V above the grounded sample, are accelerated to 1.8 keV, magnetically mass selected, deflected by 6° to eliminate fast neutrals, and then decelerated to impinge on the sample at an energy of 30–300 eV at normal incidence. At 100-eV ion energy, a typical C<sup>+</sup> current of 20 nA was obtained. This corresponds to a deposition rate of only 7 Å/h, which is impractical for thick film deposition but is ideal for *in situ* film evolution investigation. Three-stage differential pumping of the beam line enables the ion source to be operated at a pressure of  $\sim 1 \times 10^{-5}$  Torr, while the deposition chamber is maintained at  $< 7 \times 10^{-10}$  Torr.

A highly oriented pyrolytic graphite sample (HOPG, Union Carbide, Co.) in a rectangular shape with an area of about 1.5 mm<sup>2</sup> was cleaved along the basal plane in air and introduced into the UHV chamber. The Auger spectrum from this native graphite surface and throughout all experiments exhibited no adsorbed contaminants (i.e., no oxygen). For AES measurements, the sample was oriented perpendicular to the axis of a double-pass cylindrical mirror analyzer equipped with a coaxial electron gun. In this case the average electron emission angle  $\bar{\phi}$  is equal to the CMA-acceptance angle of 42.3° ( $\cos\bar{\phi} = 0.74$ ). In some cases Auger spectra were measured at 45° to the surface normal, where the analysis is more surface sensitive due to  $\cos\phi = 0.52$ .<sup>12</sup> The carbon KVV Auger transition, excited with an electron beam of 3 keV, was measured with an energy resolution of  $\Delta E/E = 0.6\%$ . In order to minimize any electron-beam influence on the carbon bonding state, the electron beam with an approximate diameter of 100  $\mu\text{m}$  was maintained at a current of 100 nA.  $N(E)E$  spectra were recorded in the pulse-counting mode; the acquisition time for one spectrum was about 320 s; these spectra were subjected to a 9-point smoothing and 5-point differentiation computer routine.

The ion (C<sup>+</sup> or Ne<sup>+</sup>) doses were measured by time integration of the current on the sample. The accuracy of such measurements was also checked using Faraday-cup profiling of the ion beam. A series of increasing ion doses were used in both C<sup>+</sup> deposition and Ne<sup>+</sup> bombardment, starting from below  $1 \times 10^{15}$  ions/cm<sup>2</sup> up to several times  $10^{17}$  ions/cm<sup>2</sup>.

## III. PRINCIPLES OF DATA EVALUATION

In order to identify the different chemical states of carbon during ion deposition, we attempted to reproduce the various measured Auger spectra by a linear combination of reference spectra. These were spectra of the native graphite surface, the (110) surface of natural diamond, a

graphite surface that was extensively bombarded with 1 and 3 kV Ar<sup>+</sup> until steady-state conditions were attained, and a thermally evaporated black carbon film. The graphite surface is known to have nearly ideal structure and has been studied as an example of the pure  $sp^2$ -bond type.<sup>13</sup> The (110) diamond surface is also nearly ideal, with no reconstruction,<sup>10</sup> and it can be considered as an example of pure  $sp^3$ -bond type. The bond states of the other two species are more uncertain. However, the requirement on a standard is only its reproducibility (unique chemical state), and this is fulfilled.

Using a linear superposition of reference Auger KVV spectra to describe the chemical state of an unknown species involves some uncertainty because of the following reasons. (1) The representation of the spectrum of a mixture of phases by a linear combination of intrinsic Auger line shapes of different standards may be correct, but the respective inelastically scattered electron contribution in the extrinsic (measured) spectrum can differ from those of the reference spectra. (2) The investigated phase may, due to its own unique valence-band electronic structure, have a different Auger line shape from the reference materials.

As far as the possibility of different loss contributions is concerned, we measured the respective electron loss spectra and constructed the intrinsic Auger line shapes. No new features of the Auger line shapes emerge due to this procedure, although the features appear better resolved. Nevertheless, the loss differences, increasing with decreasing electron kinetic energy, may contribute to the discrepancies between the measured and calculated spectra. The second objection can be removed if we remember that the Auger valence-band transition is dominantly sensitive to local electronic structure.<sup>9</sup> Consequently, it is reasonable to describe an unknown carbon phase with spectra of standards which represent, for example, the local atomic arrangements of the  $sp^2$ -hybrid bond of graphite and  $sp^3$ -hybrid bond of diamond. This description does not imply that the new phase is a mixture of graphite and diamond, but rather that its carbon bonds are of  $sp^2$  and  $sp^3$  type.

Factor analysis<sup>14</sup> was employed to determine the number of physically relevant components, i.e., different chemical states, in the sequence of C KVV spectra acquired in the course of C<sup>+</sup> and Ne<sup>+</sup> bombardment. This procedure can reveal the existence of additional chemical states. With the help of a test procedure (target transformation<sup>14</sup>), the standard spectra of several different carbon species were checked for their presence as a factor within the sequence of spectra. Those standards which test positively are identified as components. The application and mathematical procedure of both methods, least-squares decomposition and factor analysis, have been described in more detail elsewhere.<sup>15</sup>

## IV. RESULTS

### A. Ne<sup>+</sup> bombardment of graphite

A C KVV Auger spectrum of native graphite and similar spectra obtained after subsequent extensive 150-eV

Ne<sup>+</sup> and C<sup>+</sup> bombardment are shown in Fig. 1. Evolution of details of important regions of the *KVV* spectra (244–264 eV and 276–284 eV) due to gradually increasing doses of Ne<sup>+</sup> ions is shown in Fig. 2. The overall peak-to-peak height decreases with increasing Ne<sup>+</sup> dose; for comparison purposes the spectra in Fig. 2 are shown with normalized heights from base line to minimum (cf.  $I_0$  of Fig. 8). The minimum of the derivative Auger line for graphite was measured at 272.4 eV. It shifts during bombardment by 0.8–1.2 eV to higher energy; this shift is complete by a dose of  $2.7 \times 10^{15}$  ions/cm<sup>2</sup>. Changes in the spectra near the maxima at  $\sim 250$  and  $\sim 258$  eV [Fig. 2(a)] are in the relative peak heights, while a clear line-shape alteration, i.e., a shoulder growing with increasing ion dose, appears near 279 eV [Fig. 2(b)]. After a dose of  $4.1 \times 10^{16}$  ions/cm<sup>2</sup>, the line shape is no longer influenced by the Ne<sup>+</sup> bombardment. Additional doses with 300 eV Ne<sup>+</sup> lead to no further growth of this high-energy shoulder. The energy positions of the maxima of the calculated partial Auger contributions of  $\sigma^*\sigma$ ,  $\sigma^*\pi$ , and  $\pi^*\pi$  (after Ref. 13) are indicated at the top of Fig. 1 in order to assist in interpretation of the Auger line-shape alteration. The  $\sigma^*\sigma$ ,  $\sigma^*\pi$ , and  $\pi^*\pi$  notations represent the self-folded partial local electron densities of  $\sigma$  and  $\pi$  states of graphite. The indicated energy positions are relative to the Fermi level determined by the carbon 1s level binding energy.

Application of principal-component analysis as part of the factor analysis<sup>14</sup> reveals two relevant eigenvalues for the data matrix of the spectral sequences of Fig. 2. This means that the gradual change in the Auger line shape is described by two independent factors. Therefore, in the course of Ne<sup>+</sup> bombardment, only two different chemical states of carbon are distinguished. One component is obviously graphite. It is no surprise that the transformed

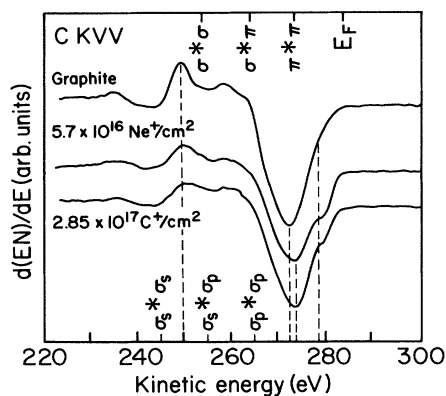


FIG. 1. C *KVV* Auger spectra of native graphite, graphite after extensive 150-eV Ne<sup>+</sup> bombardment, and graphite after extensive 150-eV C<sup>+</sup> deposition. The energy positions of the Fermi level ( $E_F$ ) and the maxima in the folded partial electron densities of  $\sigma$  and  $\pi$  states of graphite are shown at the top of the figure after Ref. 13. The energy positions of the maxima of the folded partial electron densities of diamond  $\sigma$  states are shown at the bottom of the figure after Ref. 9. The dashed lines indicate features of interest in the spectra.

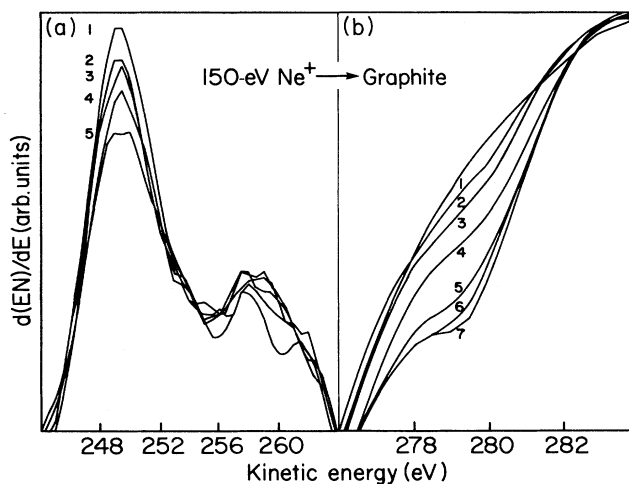


FIG. 2. Evolution of important regions of C *KVV* Auger spectra during 150-eV Ne<sup>+</sup> ion bombardment. 1, graphite; 2,  $2.4 \times 10^{14}$  ions/cm<sup>2</sup>; 3,  $4.6 \times 10^{14}$  ions/cm<sup>2</sup>; 4,  $1.0 \times 10^{15}$  ions/cm<sup>2</sup>; 5,  $2.7 \times 10^{15}$  ions/cm<sup>2</sup>; 6,  $1.1 \times 10^{16}$  ions/cm<sup>2</sup>; 7,  $4.1 \times 10^{16}$  ions/cm<sup>2</sup>.

(calculated) spectrum is in excellent agreement with the graphite spectrum [Fig. 3(a)]. The second component, although not described concretely in terms of bond type, but nevertheless identified, is heavily damaged graphite. We will refer to this component in the following as amorphous carbon (*a-C*). The good agreement [Fig. 3(b)] between the transformed spectrum and the experimental spectrum of *a-C* shows the presence of this highly disordered carbon state during low-energy Ne<sup>+</sup> bombardment. The result of a test for diamond [Fig. 3(c)] shows large discrepancies between the measured and calculated spec-

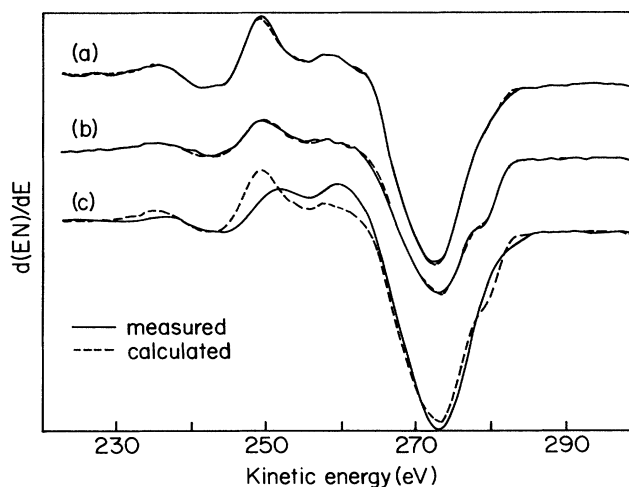


FIG. 3. Experimental and transformed Auger spectra of (a) native graphite, (b) amorphous carbon, and (c) diamond. The transformed spectra are calculated according to the target transformation procedure of factor analysis for Ne<sup>+</sup> bombardment (Ref. 14).

tra, therefore diamond cannot be considered as a possible component. Only a small amount of neon (maximum peak-to-peak ratio to carbon: 0.04) is retained in the carbon surface according to the AES data.

### B. C<sup>+</sup> deposition on graphite

The final result of the evolution of the C KVV spectra during 150-eV C<sup>+</sup> deposition is shown in Fig. 1. Details of the important regions of the spectra are shown in their course of evolution in Fig. 4. As in Fig. 2, the spectra are shown with normalized heights from base line to minimum. At doses <math>1 \times 10^{16}</math> ions/cm<sup>2</sup>, the spectra are nearly identical to those for similar doses of Ne<sup>+</sup> bombardment (Fig. 2). The maxima at ~250 and ~258 eV decrease [Fig. 4(a)], the minimum at ~272 eV shifts by 1.4 eV to higher energy (Fig. 1), and growth of a shoulder at ~279 eV can be observed [Fig. 4(b)]. In contrast to Ne<sup>+</sup> bombardment, however, C<sup>+</sup> interaction with the graphite substrate leads, after a dose of  $1 \times 10^{16}$

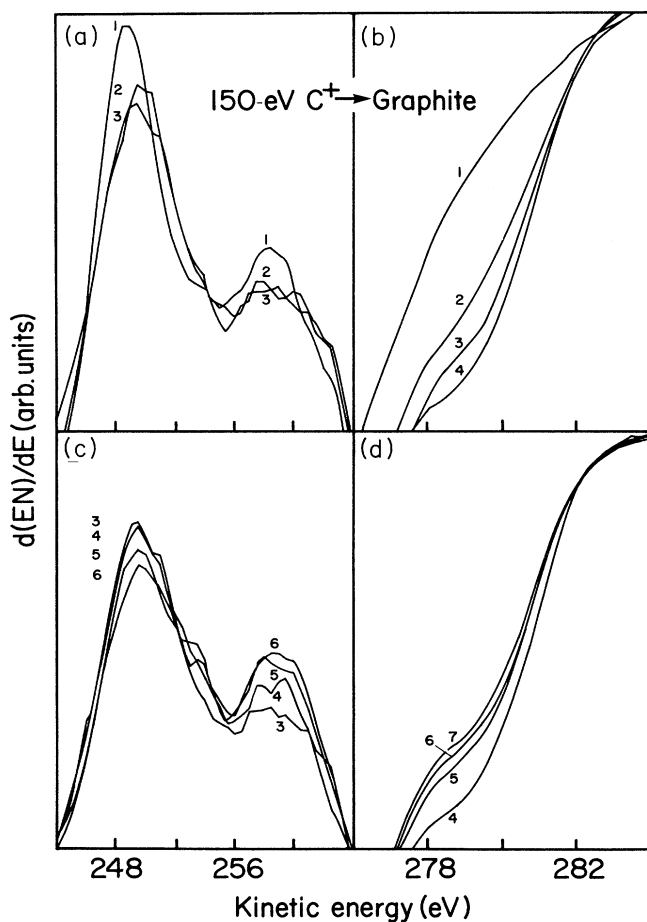


FIG. 4. Evolution of important regions of C KVV Auger spectra during 150-eV C<sup>+</sup> deposition. 1, graphite; 2,  $1.0 \times 10^{15}$  ions/cm<sup>2</sup>; 3,  $3.4 \times 10^{15}$  ions/cm<sup>2</sup>; 4,  $1.2 \times 10^{16}$  ions/cm<sup>2</sup>; 5,  $2.8 \times 10^{16}$  ions/cm<sup>2</sup>; 6,  $4.5 \times 10^{16}$  ions/cm<sup>2</sup>; 7,  $2.6 \times 10^{17}$  ions/cm<sup>2</sup>.

ions/cm<sup>2</sup>, to reversal of some of these initial changes: the intensity of the peak at ~258 eV increases [Fig. 4(c)] and the intensity of the high-energy shoulder at 279 eV decreases [Fig. 4(d)]. After a dose of  $2.7 \times 10^{17}$  ions/cm<sup>2</sup>, the line shape does not change significantly. The energy positions of the maxima of the calculated partial Auger contributions related to  $\sigma_s * \sigma_s$ ,  $\sigma_s * \sigma_p$ , and  $\sigma_p * \sigma_p$  for diamond<sup>9</sup> are shown at the bottom in Fig. 1.

Factor analysis of the sequence of spectra in Fig. 4 yields three relevant eigenvalues (factors), i.e., three different carbon chemical states. Again, it is obvious that graphite represents the first. The second component is, as for the Ne<sup>+</sup> deposition, amorphous carbon, as shown with positive target testing [Fig. 5(a)]. The third component is assumed to be the *sp*<sup>3</sup>-hybridized component represented by the spectrum of diamond; the test shows satisfactory agreement between the calculated and measured diamond spectra [Fig. 5(b)]. The small discrepancies, particularly the small high-energy shoulder in the transformed spectrum, are not considered to be significant differences [cf. the example of a negative test result in Fig. 3(c)]. Such discrepancies may be signs that the contribution of a certain component varies only during a limited number of steps of the analyzed sequence. We shall see later that this is indeed the case for the diamond contribution.

The presence of *sp*<sup>3</sup> bonds in ion-beam deposited carbon films is further confirmed by the successful least-squares decomposition of the Auger spectrum into the standard spectra of natural diamond and amorphous carbon. Figure 6 shows the superposed standard spectra with the fractions of 0.43 for the *a*-C and 0.57 for the diamond components, together with the measured spectrum (50 eV,  $3 \times 10^{17}$  C<sup>+</sup>/cm<sup>2</sup>). The agreement is satisfactory, particularly in the energy region between 250 and 265 eV where the spectra of the components exhibit major differences.

The results of the least-squares decomposition for the

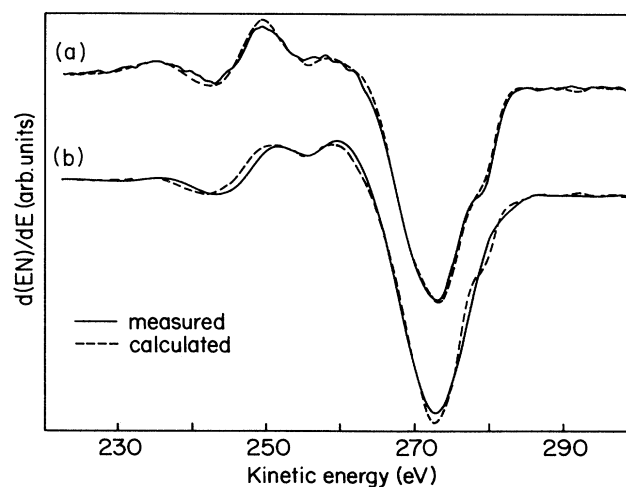


FIG. 5. Factor analysis tests of (a) amorphous carbon and (b) diamond for C<sup>+</sup> deposition as in Fig. 3.

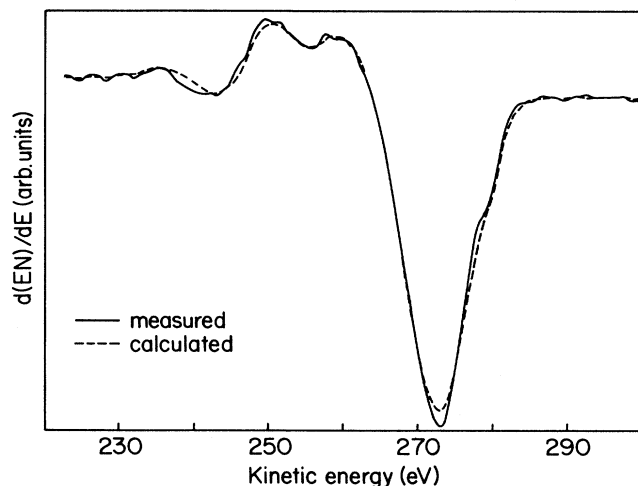


FIG. 6. Result of least-squares fitting of the C KVV spectrum of a deposited film after a dose of  $\sim 3 \times 10^{17}$   $C^+$ /cm<sup>2</sup> at 50 eV (solid line). The calculated spectrum (dashed line) is the superposition of the standard spectra of natural diamond and amorphous carbon multiplied by the fractions 0.57 and 0.43, respectively.

complete sequence of Auger spectra with  $Ne^+$  and  $C^+$  bombardment are shown in Fig. 7. For quantification of the different chemical states during ion bombardment, the standard spectra of native graphite, amorphous carbon, and natural diamond, were used. The measured overall peak-to-peak height ratios between graphite, amorphous carbon, and diamond are 1:0.7:1.8, respectively. In the  $Ne^+$  bombardment case, the standards were used according to their measured weights, represented by these peak-to-peak heights. In the  $C^+$  bombardment case, however, the weight of the amor-

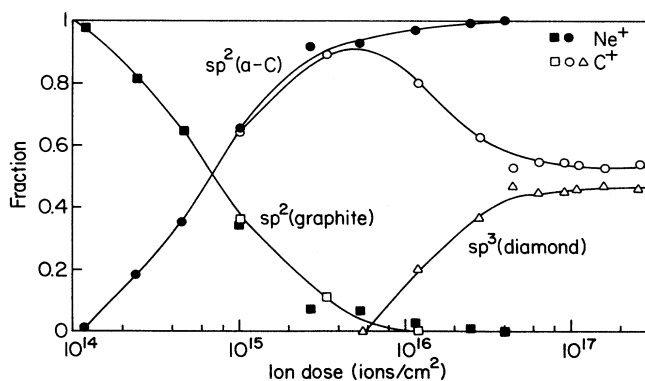


FIG. 7. Normalized fractions of the graphitic, amorphous, and diamond states of carbon during the course of the  $Ne^+$  bombardment (solid symbols) and  $C^+$  deposition (open symbols) as a function of ion dose. These are obtained by least-squares fitting of the respective standard spectra as shown in Fig. 6. The graphite, *a*-C, and diamond components are shown as squares, dots, and triangles, respectively.

phous carbon component was set equal to that of the diamond component, in order to take into account that the atomic density does not decrease (as it does due to noble gas sputtering), but rather a densification occurs.<sup>16</sup> The error of the decomposition results shown in Fig. 7 is estimated to be  $\pm 0.07$ .

The change in the chemical state of carbon in the surface region during  $Ne^+$  bombardment and during  $C^+$  deposition is clearly reflected by the profiles in Fig. 7. The graphitic state is quickly reduced with both  $Ne^+$  and  $C^+$  ions and vanishes after  $\sim 6 \times 10^{15}$  ions/cm<sup>2</sup>, while the amorphous carbon fraction strongly increases. The latter component reaches a maximum after about  $6 \times 10^{15}$  ions/cm<sup>2</sup> for carbon deposition, and then decreases due to formation and growth of an  $sp^3$ -bonded structure. The growth of this  $sp^3$ -bonded component reaches a steady-state plateau at a dose of  $\sim 8 \times 10^{16}$   $C^+$ /cm<sup>2</sup>, where the ratio of the amorphous to the diamond fraction becomes constant. In contrast to  $C^+$  deposition, no  $sp^3$ -bonded component is observed for  $Ne^+$  bombardment; only an amorphous carbon state is observed.

The dominant change in the high-energy region of the KVV Auger spectra is the shoulder (or peak) at 279 eV. We can quantify the size of this shoulder using a shape factor  $S$  defined as

$$S = I_1 / I_0, \quad (1)$$

where  $I_1$  is the ordinate in the derivative at 279 eV, measured from the base line, and  $I_0$  is the same at the peak minimum (cf. inset of Fig. 8). This shape factor allows the presentation of all of our results for both the  $Ne^+$  and  $C^+$  bombardment in the form of Fig. 8 where the ratio

$$(S - S_G) / S_G \quad (2)$$

is plotted against ion dose. Here  $S_G$  is the shape factor of the graphite spectrum. The error of the determination of the results in Fig. 8 is estimated to be  $\pm 0.09$ .

Several features of Fig. 7 are repeated in Fig. 8, showing that the emergence of the high-energy shoulder plays

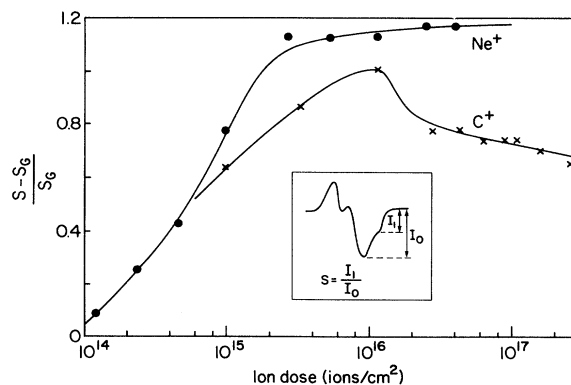


FIG. 8. Dependence of the shape factor ratio  $(S - S_G) / S_G$  on the ion dose for  $Ne^+$  ion bombardment ( $\bullet$ ) and  $C^+$  ion deposition ( $\times$ ) using 150-eV ions. The shape factor is defined as  $S = I_1 / I_0$ , where  $I_1$  and  $I_0$  are defined for each Auger spectrum as shown in the inset.

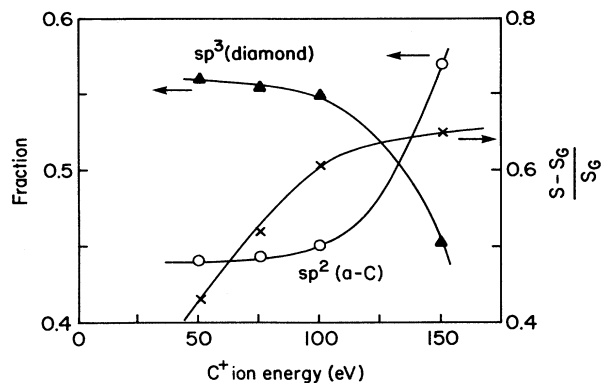


FIG. 9. Normalized diamond ( $\blacktriangle$ ) and amorphous carbon ( $\circ$ ) fractions obtained in a series of successive experiments of  $C^+$  deposition at different impact energies (from 50 to 150 eV). The change of the shape factor [cf. expressions (1) and (2)] is also shown for the same experiments ( $\times$ ).

a major role in our analysis based on least-squares decomposition. One has to conclude, therefore, that the ion-beam deposition process induces changes in those electronic states contributing to the high-energy region of the  $KVV$  spectrum, i.e., those with lower binding energy.

Upon completion of the 150-eV  $C^+$  deposition sequence (i.e., a dose of  $\sim 3 \times 10^{17} \text{ cm}^{-2}$ ), a sequence of additional depositions of small  $C^+$  doses with lower energy, i.e.,  $1.5 \times 10^{16} \text{ cm}^{-2}$  at 100 eV,  $8 \times 10^{15} \text{ cm}^{-2}$  at 75 eV, and  $5 \times 10^{14} \text{ cm}^{-2}$  at 50 eV, was carried out. As Fig. 9 shows, these steps lead to a further increase of the measured  $sp^3$ -bonded fraction. The same shape factor ratio, Eq. (2), shown in Fig. 8 is plotted in Fig. 9. Again, as the  $sp^3$ -bonded fraction observed at lower impact energies in-

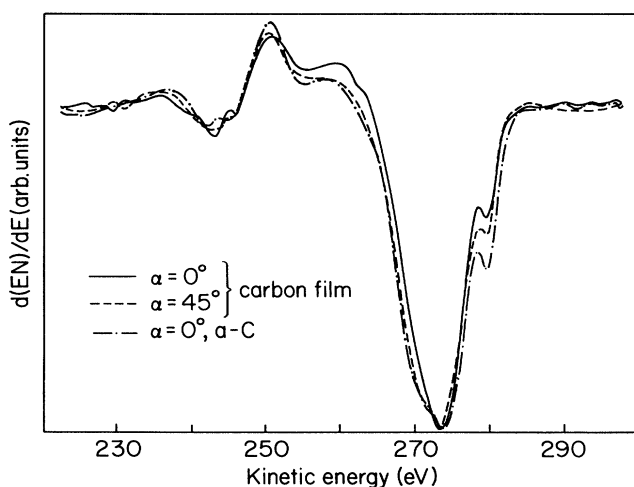


FIG. 10. C  $KVV$  spectra after 75-eV  $C^+$  deposition of ca.  $3 \times 10^{17} \text{ ions/cm}^2$  measured at two different angles  $\alpha$  between the surface normal and CMA axis. The spectrum ( $\alpha = 0^\circ$ ) of the amorphous carbon sample is also shown for comparison. All spectra are shown with normalized heights from base line to minimum.

creases, the high-energy shoulder decreases.

The angular dependence of the Auger electron escape depths provides information about the depth distribution of the chemical states. High-resolution Auger spectra of the final  $C^+$  deposited film were recorded for this purpose at  $\alpha = 0^\circ$  (surface normal) and  $\alpha = 45^\circ$  using a constant pass energy of 80 eV (energy resolution 0.48 eV; Fig. 10). For comparison, a similar spectrum of amorphous carbon is also shown ( $a-C$  spectra at  $\alpha = 0^\circ$  and  $45^\circ$  are identical). The spectrum for  $\alpha = 45^\circ$  (which gives more information about the near surface region) resembles the spectra taken in the initial state of ion deposition. The second maximum at  $\sim 258$  eV is only weakly developed and the high-energy feature at 279 eV appears now as a distinct and relatively intense peak. In contrast, in the spectrum for  $\alpha = 0^\circ$  the maximum at 258 eV is more intense and the high-energy peak is less intense.

## V. DISCUSSION

The experimental results show that carbon film growth by  $C^+$  deposition occurs in two stages. The behavior in the initial stage ( $A$ ) is characterized by phenomena which are also observed for  $Ne^+$  bombardment, i.e., the shift in the peak minimum and the development and growth of the high-energy peak in the Auger spectrum. These changes are interpreted as an increase in the amorphous carbon component (see Fig. 7). The second stage ( $B$ ) deviates from the  $Ne^+$ -graphite interaction and is characterized by the simultaneous growth of the peak at  $\sim 258$  eV and decrease of the high-energy peak. This is interpreted as formation and growth of the  $sp^3$  component (Fig. 7). The processes taking place in these two stages of film growth will now be described based upon the interpretation of the structural and chemical information available in the C  $KVV$  spectra.

### A. Defect formation

Spectral changes in the initial stage of  $C^+$  deposition ( $< 6 \times 10^{15} \text{ ions/cm}^2$ ) are due to ion-induced structural modifications only. One can arrive at this conclusion from the observation that the C  $KVV$  spectrum is nearly identical for  $Ne^+$  and  $C^+$  bombardment at this stage and the reasonable assumption that any chemical interaction between the subplanted neon and the graphite lattice can be neglected. This implies that low  $C^+$  doses of subplanted carbon do not interact chemically with the graphite lattice. The ion impact on the graphite lattice leads to growing structural disorder, which, of course, affects the electronic structure and chemical state of carbon.

The electronic structure in the valence band of graphite is described by the  $\sigma$  ( $sp^2$ ) band with the  $\sigma_s$  and  $\sigma_p$  partial density of states (DOS) and the  $\pi$  band arising from the  $p_z$  orbital overlap.<sup>17,18</sup> With the help of these local partial DOS (Ref. 18) and the application of the Cini formalism<sup>19</sup> for hole-hole interaction, Houston *et al.*<sup>13</sup> calculated the Auger line shape of graphite and found good agreement with the experiments, with the exception of the low-energy region of the line (near 240 eV). The energy positions of their self-folded partial DOS modified according to the Cini model (cf. Fig. 1) help to

point out the electronic states involved in the ion-induced damage. First, the decrease of the peak at 250 eV is proportional to the overall decrease of the peak-to-peak height, and thus it does not indicate a change in the  $\sigma$  states (the  $\sigma^*\sigma$  fold). This decrease simply results from the decrease of atomic density due to creation of vacancies. Second, the decrease of the peak at 258 eV together with the emergence of the peak at 279 eV indicate a change in the  $\pi$  states, which affects both the  $\sigma^*\pi$  and  $\pi^*\pi$  folds. This line-shape change can result from a shift of some of the  $\pi$  states to lower binding energies as a consequence of increasing disorder.

There are two forms of disorder to be considered: (1) a randomly oriented  $sp^2$ -bonded network and (2) point defects. The point defects may be both vacancies and interstitials, but there is no reason to expect a significant difference in the electronic structure resulting from vacancies and interstitials.

Any disorder in the graphite lattice disturbs the optimal  $p_x-p_z$  orbital overlap. This leads to a narrowing of the pseudo-band-gap of graphite and to electronic levels near the Fermi level. In other words, the separation of the  $\pi$  (bonding) and  $\pi^*$  (antibonding) bands is reduced due to defect creation. This is in agreement with the calculated DOS for a random  $sp^2$ -carbon network which shows a smooth distribution of the  $\pi$  electronic states below and near the Fermi level.<sup>20</sup> Such a change of the  $\pi$  electron DOS may be responsible for the 1.4-eV shift of the Auger line to higher energy and also for the peak  $\sim 3.8$  eV below the Fermi level (Fig. 1).

Electronic states near the Fermi level may arise also due to point defects with nonbonding orbitals ( $s$  and  $p$  characters). Such point defects are readily created either as interstitials (due to knock-on in the case of  $Ne^+$  ions and also due to subplantation in the case of  $C^+$  ions) or as vacancies (due to knock-on in both cases). The first stage of  $C^+$  deposition ( $< 6 \times 10^{15}$  ions/cm<sup>2</sup>) is therefore characterized by an increasing number of point defects which results in growing disorder toward an amorphous structure (cf. Figs. 7 and 8). The existence of a high-energy peak has been observed in some previous studies<sup>21,22</sup> and Khvostov *et al.*<sup>23</sup> have interpreted it as a contribution of the  $\pi^*\pi$  fold. In their interpretation, however, the binding energy of the  $\pi^*\pi$  fold is unchanged during transformation of a diamondlike amorphous carbon due to annealing, the only change being an increase in the  $\pi$  DOS. While this does not conflict with our interpretation, it is important to point out that consideration of a binding energy shift is necessary to interpret the transition from HOPG to  $a$ -C.

The high stability of hexagonal carbon rings with  $sp^2$  hybridization<sup>20</sup> could guarantee the survival of graphitic clusters embedded in an interconnecting network, even after ion bombardment. There is considerable evidence that amorphous carbon consists of small randomly oriented graphitic clusters with  $sp^2$  sites which are interconnected partially by tetrahedrally coordinated atoms ( $\sim 95\%$   $sp^2$ ,  $\sim 5\%$   $sp^3$  bonds).<sup>24,25</sup> We assume that the  $Ar^+$  bombarded graphite is essentially the same material considered by these authors. Consequently, amorphous carbon as a fractional component in Fig. 7, does not

represent a distinct chemical state with respect to graphite but rather a degree of disorder.

As a result of the above considerations we can now construct a simple model of the carbon structure in the initial stages of ion-beam deposition with symbolized structural elements, as shown in Figs. 11(a) and 11(b). The structure in Fig. 11(a) corresponds to small ion doses, where the lattice damage of graphite is restricted to formation of vacancies and interstitials. In a later stage the structure is a partially randomized network of mainly hexagonal and also some odd-numbered carbon rings, complemented with vacancies and interstitials [Fig. 11(b)]. In the beginning, the graphitic elements may be preferentially oriented parallel to the initial basal planes.

The chemical and structural state described in the initial stage of  $C^+$  ion deposition on graphite may be similar to the intermediate stage of carbon deposition on various metal and semiconductor substrates like Ni, Si, etc. Following a carbide formation stage, an intermediate stage in which Auger spectra similar to those observed here at about  $1 \times 10^{16}$  ions/cm<sup>2</sup> is usually observed.<sup>7</sup> It appears therefore that this carbon-layer structure comprising randomly oriented  $sp^2$  bonds and a significant number of point defects is of unique character and can be achieved either by damaging the graphite lattice or by the buildup of a carbon phase due to ion-beam deposition.

At higher ion doses ( $> 6 \times 10^{15}$  ions/cm<sup>2</sup>) the effect of  $Ne^+$  and  $C^+$  bombardment becomes markedly different (cf. Figs. 7 and 8). In the case of  $Ne^+$ , an even more complete destruction of the original graphite lattice is observed, while the additional  $C^+$  doses result in an apparent change into the development of another phase.

## B. Network formation

In contrast to neon, the subplanted carbon interacts chemically with neighboring atoms at high doses. After a dose of ca.  $1 \times 10^{16}$  ions/cm<sup>2</sup>, the high-energy peak at 279 eV decreases simultaneously with an increase of the maximum at 258 eV (cf. Figs. 4 and 8) along with the formation and growth of the  $sp^3$ -bond fraction (Fig. 7). We suggest that these changes are related in the following way: carbon interstitials begin to form new bonds with their neighboring atoms in a tetrahedral configuration, i.e.,  $sp^3$ -bond type.

The  $KVV$  Auger line of diamond results from a valence band in which the  $\sigma_p^*\sigma_p$  fold constitutes  $\sim 75\%$  of the DOS.<sup>9</sup> One of the consequences of this situation is that the minimum of the derivative Auger spectrum is approximately at the same position as in graphite, in spite of the missing  $\pi^*\pi$  fold. This is unfortunate because a line shift would be an easily recognizable sign of diamond formation. Another consequence is, however, that the maximum at  $\sim 258$  eV in the Auger spectrum is relatively high, reflecting a steep rise in the direct spectrum preceding the  $\sigma_p^*\sigma_p$  maximum (cf. the positions indicated in Fig. 1 following Ref. 9). This is why this maximum is a sensitive indicator of the presence of  $sp^3$  bonds. The graphite  $\sigma^*\pi$  fold is close to the energy of the diamond  $\sigma_p^*\sigma_p$  fold; thus a small maximum is also present at this energy in the graphite spectrum.

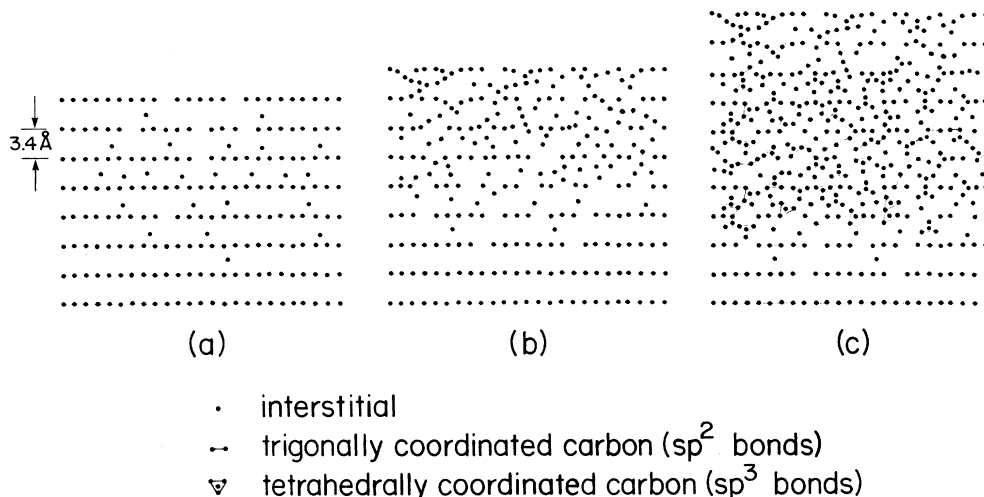


FIG. 11. Models of structural arrangements for the defect creation (a) and (b) and network formation (c) stages of carbon deposition on graphite. The initial stage (a) is characterized by the subplantation of carbon atoms in interstitial sites between the planes of hexagonal carbon rings and displaced atoms leaving vacancies. Later (b), the graphite planes become heavily damaged and the structure is a partially randomized  $sp^2$  network. Subsequently (c), tetrahedrally coordinated atoms and trigonally coordinated clusters of the damaged basal planes form a composite  $sp^3$ - $sp^2$  network. The surface evolves outward during these processes.

The decrease of the high-energy peak at 279 eV when high  $C^+$  doses ( $> 1 \times 10^{16}$  ions/cm<sup>2</sup>) are applied must be related to the decrease in the number of those low binding energy  $\pi$  and nonbonding states described in the preceding section. This process is not a simple reversal of the defect creation, but involves a net decrease in the number of  $\pi$  states and a corresponding increase in the number of  $sp^3$ - $\sigma$  states. The energy position of the high-energy peak does not change because this process involves only the change of the number of  $\pi$  states, not a shift in their binding energy, similar to that described in Ref. 23.

The diamond structure is a close-packed lattice, i.e., it accommodates more atoms per unit volume than other arrangements. It is suggested then that, as the carbon atomic density is increased due to retention of more and more  $C^+$  ions, a new phase of tetrahedrally arranged carbon forms.

This process is illustrated in Fig. 11(c) with a model of the structural arrangement during the later stages of carbon deposition. The graphite basal planes are heavily damaged in the upper surface region to the extent that only graphitic clusters remain. The deposited carbon is able to form bonds with these clusters at perimeter sites. The forced enrichment of carbon atoms in interstitial sites makes the interconnection between them also possible. Consequently, an  $sp^3$  network is formed which interconnects the graphitic clusters [Fig. 11(c)]. With respect to the subplantation model,<sup>8</sup> atoms with lower binding energy are preferentially displaced leading in this case to an increasing fraction of  $sp^3$  bonds at the expense of  $sp^2$  bonds.

As indicated in Fig. 11, there is a depth distribution in both the defect and network formation processes. The incoming ions penetrate the top surface layers where they

can create defects by collisions before they are thermalized. The resulting energy-dependent penetration range for 150- and 50-eV  $C^+$  as calculated with the Biersack-Ziegler Monte Carlo computer program code (TRIM89, Ref. 26) are shown in Fig. 12. The target in these calculations is amorphous and we use the results only to illustrate the depth dependence of defect and network formation in comparison with the information depth of AES. It follows from Fig. 12 that for 150-eV  $C^+$ , the accumulation of subplanted carbon peaks near a depth of  $\sim 9$  Å where many  $sp^3$  bonds are formed. In the region closer

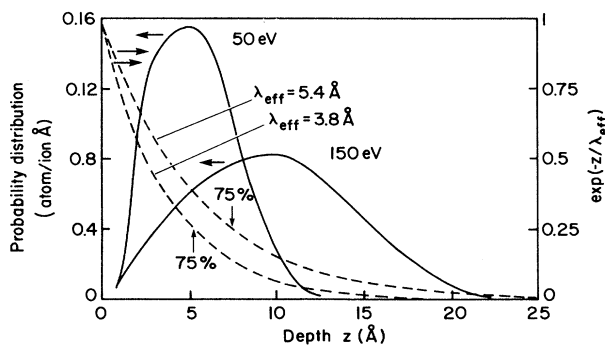


FIG. 12. Depth profile of subplanted 50- and 150-eV  $C^+$ , as calculated from TRIM 89 (Ref. 26). The ordinate is the probability with which  $C^+$  is stopped at a certain depth below the surface. Also shown is the function  $\exp(-z/\lambda_{\text{eff}})$  for escape depths  $\lambda_{\text{eff}} = 5.4$  Å ( $\alpha = 0^\circ$ ) and  $\lambda_{\text{eff}} = 3.8$  Å ( $\alpha = 45^\circ$ ), which represents the depth-dependent fraction of the Auger signal. The respective marks give the depth from which 75% of the total signal is obtained. The inelastic mean free path of the electrons is  $\lambda = 7.3$  Å from Ref. 27.

to the surface, the influence of collisional damage is stronger, maintaining a higher  $sp^2$ -bond fraction even after high ion doses. This means that the model of Fig. 11(c) describes the steady-state situation with constant  $sp^2/sp^3$  ratio after  $\sim 1 \times 10^{17}$  ions/cm<sup>2</sup> (cf. Fig. 7). If the ion energy is decreased to 50 eV, the subplanted carbon enriches at a depth of  $\sim 5$  Å, with the formation of more  $sp^3$  bonds closer to the surface. When we examine these surfaces by AES we must be aware that 75% of the spectral intensity comes from a depth of 7.5 Å for  $\alpha=0^\circ$  and 5.3 Å for  $\alpha=45^\circ$ . This is illustrated by the  $\exp(-z/\lambda_{\text{eff}})$  curves in Fig. 12, where  $z$  is the depth and  $\lambda_{\text{eff}}$  is the escape depth of the C  $KVV$  Auger electrons. There are two consequences of the above depth dependences. First, the observed angular dependence (Fig. 10), where the spectrum for  $\alpha=0^\circ$  represents mainly the  $sp^3$ -network formation in a deeper region and the spectrum for  $\alpha=45^\circ$  reflects the situation nearer the surface with more damage (note the more intense peak at 279 eV for  $\alpha=45^\circ$ ). Second, this depth dependence of the  $sp^2$ - to  $sp^3$ -bond ratio affects, of course, the quantification of the different carbon component fractions during ion deposition (Fig. 7). This decomposition procedure is obviously only correct for a homogeneous distribution of the components and the fraction of the deeper-lying component is underestimated. If one had precise information for both the ion-stopping distribution and electron-escape depth, i.e., both types of curves in Fig. 12, then a true fractional composition could be derived. Nevertheless, Fig. 7 properly characterizes the trends of the development of the different carbon component fractions.

$sp^3$ -bond fractions observed at lower  $C^+$  ion impact energies (Fig. 9) are less underestimated because of lower subplantation depth. This effect can completely account for the observed decrease of defect structure and increase of  $sp^3$ -bond fraction at lower carbon impact energies. There is no need to assume a different mechanism which would result in lower damage and a higher level of  $sp^3$ -bond formation at lower impact energies, even though such effects may take place.

There are dense carbon arrangements other than diamond. In fact,  $sp^2$  bonds are shorter than  $sp^3$  bonds. It is therefore possible that some of the carbon atoms at high deposition doses will form  $sp^2$  interconnections.

Such effects could account for the decrease of the high-energy shoulder above a dose of  $6 \times 10^{16}$  ions/cm<sup>2</sup> when the  $sp^3$ -bond fraction is already saturated (cf. Figs. 7 and 8). The very complex nature of the carbon film structure resulting from ion-beam deposition may be responsible for the fact that attempts for direct determination of such structures via diffraction techniques have been unsuccessful to date.

## VI. CONCLUSIONS

Detailed analysis of the C  $KVV$  Auger spectra acquired after  $C^+$  deposition and complemented with  $Ne^+$  bombardment experiments on graphite constitute an approach to the problem of *in situ* diagnostics of the results of low-energy  $C^+$  deposition. The following main conclusions can be drawn from this work.

1. Carbon film evolution occurs in two stages: (i) the initial defect creation including damaging the graphite lattice and introduction of point defects (interstitials and vacancies) and (ii) the buildup of a network with the formation of  $sp^3$ -hybrid bonds. The final  $C^+$  deposited carbon film can be considered as a network of tetrahedrally and in part trigonally coordinated carbon atoms with  $sp^3$ - and  $sp^2$ -hybrid bonding, respectively.

2. The dose-dependent variation of the  $sp^3$ - and  $sp^2$ -bond fractions is verified by successful application of a least-squares decomposition of the Auger spectra.

3. The high-energy peak in the C  $KVV$  Auger spectrum reveals the existence of defects which give rise, due to their nonaligned  $\pi$  orbitals or nonbonding states, to a DOS at low binding energies.

4. The  $sp^2$ -bond fraction is higher near the surface while more  $sp^3$  bonds are formed in deeper layers, in accord with the subplantation model.

## ACKNOWLEDGMENTS

This material is based on work supported by the National Science Foundation under Grant No. DMR-89-14608. C.D.R. gratefully acknowledges partial support from IBM.

<sup>1</sup>J. W. Rabalais and S. Kasi, *Science* **239**, 623 (1988).

<sup>2</sup>C. Weissmantel, in *Thin Films From Free Atoms and Particles*, edited by K. J. Klabunde (Academic, Orlando, Florida, 1985), Chap. 4.

<sup>3</sup>H. Tsai and D. B. Bogy, *J. Vac. Sci. Technol. A* **5**, 3287 (1987).

<sup>4</sup>C. Weissmantel, E. Ackermann, K. Bewilogua, G. Hecht, H. Kupfer, and B. Rau, *J. Vac. Sci. Technol. A* **4**, 2892 (1986).

<sup>5</sup>J. E. Greene, *Solid State Technol.* **April**, 115 (1987).

<sup>6</sup>*Proceedings of the First International Symposium on Diamond and Diamond-Like Films*, edited by J. P. Dismukes, A. J. Purdes, K. E. Spear, B. S. Meyerson, K. V. Ravi, T. D. Moustakas, and M. Yoder (The Electrochemical Society, Pennington, New Jersey, 1989).

<sup>7</sup>S. R. Kasi, H. Kang, and J. W. Rabalais, *J. Chem. Phys.* **88**, 5914 (1988).

<sup>8</sup>Y. Lifshitz, S. R. Kasi, and J. W. Rabalais, *Phys. Rev. B* **41**, 10468 (1990).

<sup>9</sup>D. E. Ramaker, *J. Vac. Sci. Technol. A* **7**, 1614 (1989).

<sup>10</sup>P. G. Lurie and J. M. Wilson, *Surf. Sci.* **65**, 453 (1977); **65**, 476 (1977).

<sup>11</sup>H. Kang, S. R. Kasi, and J. W. Rabalais, *J. Chem. Phys.* **88**, 5882 (1988).

<sup>12</sup>S. Hofmann, in *Practical Surface Analysis by Auger and X-Ray Photoelectron Spectroscopy*, edited by D. Briggs and M. P. Seah (Wiley, Chichester, England, 1983), Chap. 4.

<sup>13</sup>J. E. Houston, J. W. Rogers, Jr., R. R. Rye, F. L. Hutson, and

- D. E. Ramaker, *Phys. Rev. B* **34**, 1215 (1986).
- <sup>14</sup>E. R. Malinowski and D. G. Howery, *Factor Analysis in Chemistry* (Wiley, New York, 1980).
- <sup>15</sup>S. Hofmann and J. Steffen, *Surf. Interf. Anal.* **14**, 59 (1989).
- <sup>16</sup>A. Anttila, J. Koskinen, M. Bister, and J. Hirvonen, *Thin Solid Films* **136**, 129 (1986).
- <sup>17</sup>R. F. Willis, B. Fitton, and G. S. Painter, *Phys. Rev. B* **9**, 1926 (1974).
- <sup>18</sup>J. S. Murday, B. I. Dunlap, F. L. Hutson II, and P. Oelhafen, *Phys. Rev. B* **24**, 4764 (1981).
- <sup>19</sup>M. Cini, *Solid State Commun.* **24**, 681 (1977).
- <sup>20</sup>J. Robertson and E. P. O'Reilly, *Phys. Rev. B* **35**, 2946 (1987).
- <sup>21</sup>T. J. Moravec and T. W. Orent, *J. Vac. Sci. Technol.* **18**, 226 (1981).
- <sup>22</sup>M. Dayan and S. V. Pepper, *Surf. Sci.* **138**, 549 (1984).
- <sup>23</sup>V. V. Khvostov, M. B. Guseva, V. G. Babaev, and O. Yu. Rylova, *Surf. Sci.* **169**, L253 (1986).
- <sup>24</sup>D. F. R. Mildner and J. M. Carpenter, *J. Non-Cryst. Solids* **47**, 391 (1982).
- <sup>25</sup>D. Beeman, J. Silverman, R. Lynds, and M. R. Anderson, *Phys. Rev. B* **30**, 870 (1984).
- <sup>26</sup>J. F. Ziegler, J. P. Biersack, and U. Littmark, *The Stopping and Ranges of Ions in Matter* (Pergamon, Oxford, 1985), Vol. 1.
- <sup>27</sup>S. Tanuma, C. J. Powell, and D. R. Penn, *Surf. Interf. Anal.* **11**, 577 (1988).